Draft version April 25, 2026

Typeset using LaTeX **twocolumn** style in AASTeX631

Lab 7: Photometry and a CMD

James Watt, Lab Group: Jackson Lyle, Aanya Bhandari, Sara Grinbaum

(Dated: 25^{th} April, 2026)

ABSTRACT

In lab 7 we preform the full BVRI photometric analysis of two open clusters, NGC884 and the Orion Nebula Cluster (ONC). We use data we collected over two observing nights at CTO through the 11-inch and 14-inch telescopes for NGC884 and the ONC respectively. Building on the data reduction pipeline we developed in Lab 4, which we used to reduce and produce color images of these two targets, we add a new pipeline for aperature photometry and CMD isochrone age constraining. Specifically, we use errors propagated through the data reduction pipeline and the master frames it produced to preform aperature photometry on every significant source in each image, zero-point calibration to measure their obsevred magnitudes, analyzed the sky-brightness and the seeing, as well as plotted the measured magnitudes against measured color to create color-magnitude diagrams (CMD). With the CMDs, we overplotted standard isochrones of known stellar population ages to estimate the ages of the clusters based on where their main sequence extends and where the red giant branch stars. The resulting photometry measured the magnitudes in B, V, R, and I for all 600 sources between the two targets to within 0.1-0.3 mag of their catalog confirmed values. The sky brightness across the two nights was measured to be within 19.6 and 22.9 mag arcsec^2 acorss all four filters. We recovered the read noise and dark current of the detector to be ~ 14.8 e$^-$/pixel and $\lesssim 0.06$ e$^-$/pixel/s respectively. Finally, we constrained the age of NGC884 to 10-30 Myr and the ONC to $\leq$10 Myr. Errors resulting from nearest-neighbour star identification and a corse subset of isochrones wide age constraints and outlying test star magnitude verification. Overall, this lab provided us with valuable experience building and preforming aperture photometry to measure the magnitudes of stars in certain bands as well as constrain the ages of stellar clusters.

1. INTRODUCTION

The color-magnitude diagram (CMD) is one of the most powerful tools in stellar astrophysics. BY plotting each star in a population by its apparent magnitudes in one filter against its color, the CMD can present the temperatures and luminosities of entire stellar populations in one plot. For populations such as open star clusters, the stars do not scatter randomly across the magnitude-color space, instead, they trace our a curve, isochrone, whose shape is set by the clusters age, metallicity, and stellar massesA. Bressan et al. (2012).. By comparing observed isochrones to simulated isochrones with known cluster parameters, we can estimate the age and metallicity of a given cluster. These age and cluster characteristics estimates give us a window to study stellar evolution, star formation in our galaxy, and how stellar populations evolve together.

In this lab we use our observations from CTO of two open star clusters in BVRI to construct CMDs for each cluster: NGC884, with a reported age of $\sim$ 14 Myr T. Currie et al. (2010), and the Orion Nebula Cluster (ONC), an embedded cluster with a reported age of $\sim$ 1–3 Myr L. A. Hillenbrand (1997). These two target happen to be good examples of two clusters who occupy different evolutionary regimes. NGC884 is old enough that some of its stars have begun to turn off on the main sequence towards the red giant branch. The ONC, in contrast, is a very young cluster embedded in the Orion Molecular cloud and many of its stars are stil contracting onto the main sequence from pre-main-sequence tracks. The difference between these clusters highlights how isochrone fitting accuracy differs between very young and quite old stellar populations.

This lab directly builds on the data reduction pipeline and RGB image creation done in Lab 4. Each cluster was observed in B, V, R, and I, and the raw frames were calibrated with matching dark, bias, and flat frames and aligned together with full per-pixel uncertainty propagation throughout. We then preformed aperture photometry on every non-saturated Gaussian source detected in the V image of each cluster (V band had the highest SNR) on the images in each band. This yielded sets of flux measurements for all significant stars in each cluster. These fluxes were calibrated with to apparent magnitude by using per-filter zero-points derived from a set of selected standard stars in each frame (Tycho-2 and APASS DR9 were used to retrieve absolute magnitudes of standard stars). The resulting calibrated photometry was then used to calculate the colors of each source and then construct a CMD and color-color diagram for each cluster. Finally, the CMDs made from our observed data were overlayed on theoretical PARSEC isochrones to estiamte cluster ages.

Beyond the age estimates, this lab allowed us to develop the ability to preform a full photometric work flow, mirroring that using in modern observational astronomy: per-pixel uncertainty propogation, photometric calibration against published standards, sky-background measurement, and seeing calculations. These skills we built throughout this lab directly support the more advanced photometric work we are likely to do in Obs Tech 2 or future research applications.

2. METHODS

NGC 884 was observed on 2026-02-10 with the 11-inch telescope at the Campus Teaching Observatory (CTO) through the BVRI + Clear filter set. Exposure times were 10 s in B, V, and R; 15 s in I; and 5 s in Clear, with 10 frames in each filter. During the observation the cluster was at altitude $\sim 55°$, azimuth $\sim 331°$, and airmass 1.22. Conditions were clear with little moon glow – the moon was sufficiently far from the target and faint enough to not contribute meaningfully to the sky background.

The ONC was observed on 2026-01-27 with the 14-inch telescope. Exposure times were 10s for B and 7 s for V, R and I, with 10 frames per filter, and 20 5 s frames through the clear filter. During the observations, the cluster was at an altitude of $\sim 55°$, azimuth $\sim 184°$, and airmass 1.22. The moon was not above the horizon during the observation.

The tabulated observing log is located in Table 1. Alt, Az, and Airmass calculations were calculated for the object at the time of observation (taken from fits header) considering the lat and long of CTO.

The reduction pipeline and photometry/CMD pipeline were implemented in Python using astropy, photutils, astroquery, and astroalign libraries for astrophysical tasks, and os, glob, numpy, pandas, matplotlib, and tkinter libraries for data storage, calculation, or representation.

2.1. *Image reduction and per-pixel uncertainty*

Image reduction utilized the same data reduction pipeline developed during lab 4, applied to the cluster data. Calibration followed creating a master bias, mean of bias frame stack; a master dark per exposure time, the mean of bias-subtracted dark frames; a master falt per filter, mean of bias and dark subtracted, median normalized flat frame stacks. Calibrated science images were then created by subtracting bias and dark contributions then dividing by the flat frame. Master science frames in each filter were created by using astroalign to align subframes, which were stacked and the median gave the master frame.

Per-pixel uncertainty was propagated through both the reduction and photometry pipelines. Bias and dark uncertainty scale as $\sigma/\sqrt{n}$ for n frames stacked. Flat uncertainty including source Poisson noise was propagated with bias, dark, and light by adding them in quadrature. Division by the flat term is propageted following

$$\sigma_C = |C|\sqrt{(\sigma_N/|N|)^2 + (\sigma_{\hat{f}}/|\hat{f}|)^2}, \tag{1}$$

where N is the bias- and dark-subtracted numerator. Representativ V-band uncertainty maps and their pixel-value distributions are shown in Figure 1. Most pixels in both clusters have V-band uncertainty between roughly 5 and 30 ADU per stacked frame, consistent with the expected combination of read noise (Section 2.2) and photon shot noise from the sky.

2.2. *Detector characterization*

The read noise is calculated by the standard deviation of a single bias frame multiplied by the detector gain ($g = 3.99$ e$^-$/ADU for the ASI294MM Pro). The dark current is estimated to be linear and calculated as the

Table 1. Observing log + calibration data used in the reduction. Lights are summarised per filter (geometry alt/az/airmass averaged over the 10-frame stack). Bias, dark, and flat sets are summarised below for each cluster. All frames were taken with the ZWO ASI294MM Pro at bin 4, gain 0; CCD setpoint was −5°C across all exposures.

Target	Frame	Filter	$t_{\rm exp}$ (s)	N	Alt (°)	Az (°)	Airmass
NGC 884 – 11-inch telescope, UT 2026-02-10							
NGC 884	Light	B	10.0	10	55.18	331.29	1.218
NGC 884	Light	V	10.0	10	54.99	331.01	1.221
NGC 884	Light	R	10.0	10	54.79	330.73	1.224
NGC 884	Light	I	15.0	10	54.55	330.41	1.228
NGC 884	Light	Clear	5.0	10	55.33	331.50	1.216
NGC 884	Bias	—	0	10	—	—	—
NGC 884	Dark[a]	—	0.001 – 15 (11 set)	10 each	—	—	—
NGC 884	Flat	B	0.65	10	—	—	—
NGC 884	Flat	V	0.90	10	—	—	—
NGC 884	Flat	R	1.0	10	—	—	—
NGC 884	Flat	I	3.0	10	—	—	—
NGC 884	Flat	Clear	0.30	10	—	—	—
ONC – 14-inch telescope, UT 2026-01-27							
Orion	Light	B	10.0	10	54.87	185.07	1.223
Orion	Light	V	7.0	10	54.90	184.36	1.222
Orion	Light	R	7.0	10	54.94	183.13	1.222
Orion	Light	I	7.0	10	54.92	183.74	1.222
Orion	Light	Clear	5.0	20	54.96	182.39	1.221
Orion	Bias	—	0	10	—	—	—
Orion	Dark[b]	—	0.004 – 45 (9 set)	5–10 each	—	—	—
Orion	Flat	B	15.0	3	—	—	—
Orion	Flat	V	4.0	3	—	—	—
Orion	Flat	R	1.5	3	—	—	—
Orion	Flat	I	5.0	3	—	—	—
Orion	Flat	Clear	1.0	3	—	—	—

[a]NGC 884 dark exposure times: 0.001, 0.003, 0.005, 0.15, 0.3, 0.35, 0.5, 2.5, 5, 10, 15 s (10 frames each).
[b]ONC dark exposure times: 0.004, 0.02, 0.05, 0.7, 1, 5, 7, 10, 45 s (5 frames each, except 10 frames at 10 s).

linear accumulation over time between the mean of the shortest bias subtracted dark and longest.

$$D = \frac{\bar{M}_{long} - \bar{M}_{short}}{t_{long} - t_{short}}. \tag{2}$$

2.3. *Source detection and aperture photometry*

Sources (stars) are detected using each cluster's V-band master frame with the photutils.detection.DAOStarFinder tool with a 6 σ detection threshold, and each star with a corresponding FWHM measurement to measure the V-band seeing. Saturated stars (peak pixel above 55,000 ADU) are excluded. V-band was selected for source detection as the V-band SNR was the highest as a result of the V-band's highest transmission and the V-band peak detector QE. Forced circular aperture photometry was then performed at the same pixel positions in B, R, and I, using an aperture radius $r_{ap} = 1.3 \cdot \mathrm{FWHM}_V$. Sky background is calculated as the sigma-clipped global median per filter and the per-aperture flux is thus given by,

$$F = \sum_{i \in \mathrm{ap}} I_i - A_{ap} \cdot s_{med}, \tag{3}$$

with A_{ap} the aperture pixel area and s_{med} the median sky flux. Per-pixel uncertainties are then propagated through the aperture sum to give the per-star flux uncertainty.

2.4. *Photometric calibration*

Instrumental magnitudes are

$$m_{\rm inst} = -2.5 \log_{10}(F/t_{exp}), \tag{4}$$

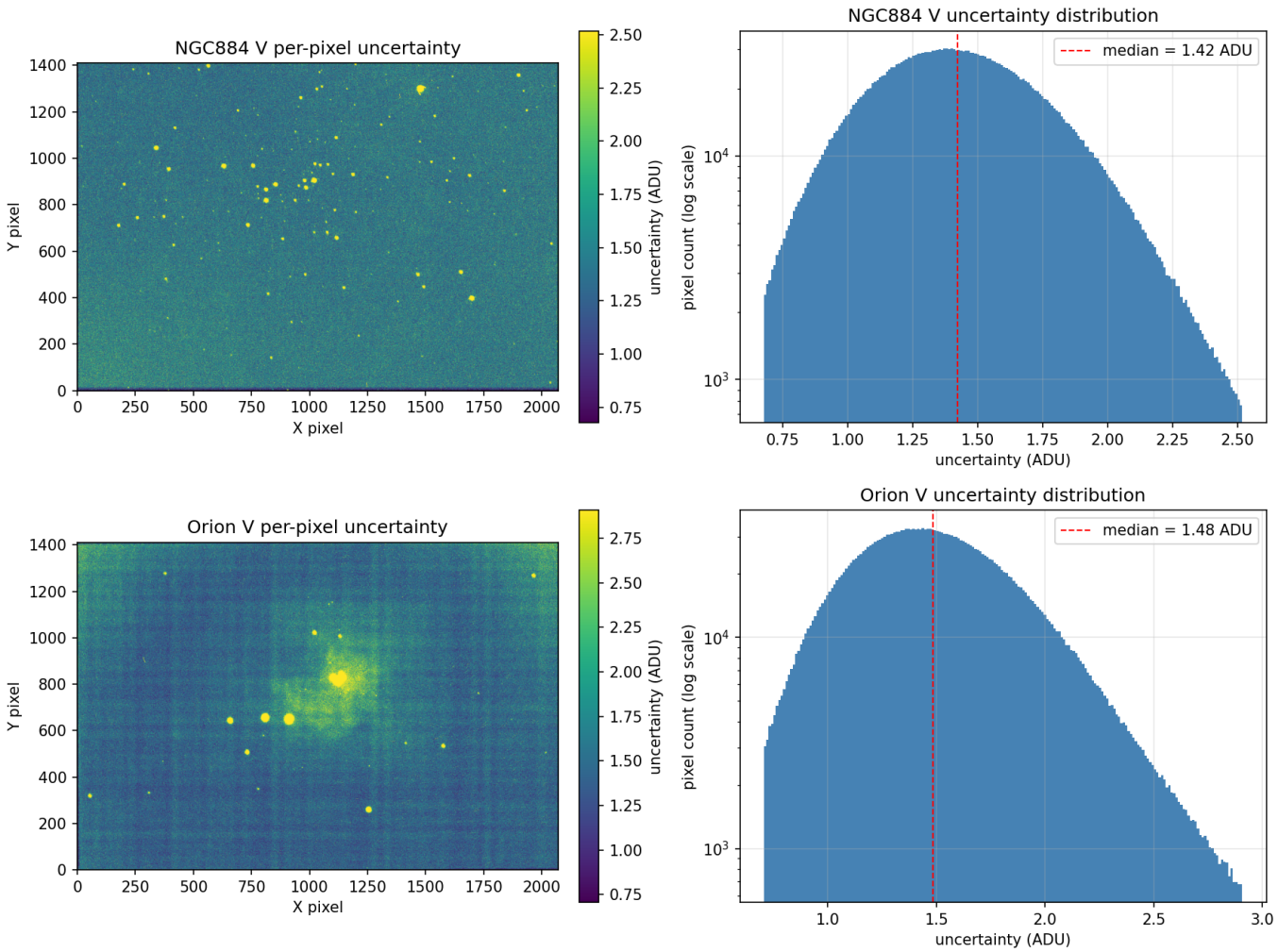


Figure 1. Per-pixel uncertainty in the V-band reduced master frames for NGC 884 (top) and the ONC (bottom). Histograms of pixel uncertainties (log-y), with the median marked are on the right.

and the per-filter zero-point is

$$m_{zp} = \langle m_{\rm cat} - m_{\rm inst} \rangle \tag{5}$$

averaged over a set of standard stars.

Standard stars were selected by labeling the brightest 20 sources in each image with an index 0-19, then plate solving the V-band master images for each cluster to identify the catalog code of 4 standard stars for each frame. For each star the Tycho-2 ID was recorded and used to identify their catalog magnitude from the Vizier catalog, prioritising APASS DR9 A. A. Henden et al. (2015) (Johnson B, V + Sloan g', r', i') when available, and falling back to Tycho-2 E. Høg et al. (2000) BT, VT converted to Johnson via the ESA transform:

$$V_J = V_T - 0.090\,(B_T - V_T), \tag{6}$$
$$B_J = V_J + 0.850\,(B_T - V_T). \tag{7}$$

APASS Sloan r', i' are converted to Cousins R, I via the Lupton (2005) SDSS EDR transforms:

$$R_C = r' - 0.2936\,(r' - i') - 0.1439, \tag{8}$$
$$I_C = r' - 1.2444\,(r' - i') - 0.3820. \tag{9}$$

Catalogue BVRI for each calibrator are listed in Table 2. Four calibrators were used for NGC 884; three were used for the ONC. For NGC 884 R and I, only one of the four calibrators was faint enough to be in APASS (Tycho does not report R, I), and thus we have only one R/I calibrator for NGC 884. See Section 4 for a discussion of the errors this presents.

2.5. *Sky brightness*

The per-filter sky brightness was computed by taking the median of all pixels with intensity below the 40th percentile of pixel value. Converting from ADU per pixel

Table 2. Tycho-2 calibrator stars and their Johnson–Cousins BVRI from APASS DR9 + Tycho-2.

Cluster	TYC ID	RA, Dec (°)	B	V	R	I	Source
NGC 884	3694-1862-1	35.249, +57.158	10.40	7.99	—	—	APASS B / Tycho V
NGC 884	3694-2332-1	35.282, +57.167	9.70	9.53	—	—	Tycho B,V
NGC 884	3694-2081-1	35.431, +57.126	9.72	9.49	—	—	Tycho B,V
NGC 884	3694-2350-1	35.704, +57.154	10.43	10.11	9.95	9.60	APASS BV + Sloan→Cousins
Orion	4774-849-1	83.791, −5.465	8.51	8.45	8.30	8.11	APASS BV + Sloan→Cousins
Orion	4774-866-1	83.960, −5.476	10.33	10.80	10.51	10.57	APASS BV + Sloan→Cousins
Orion	4774-810-1	83.708, −5.312	11.14	10.54	10.11	9.56	APASS BV + Sloan→Cousins

to magnitudes per pixel was done with the same zero-point offsets calculated earlier, and were then converted to magnitudes per arcsec^2 given our plate scale:

$$\mu_{sky} = -2.5\log_{10}(s_{med}/t_{exp}) + m_{zp} + 2.5\log_{10}(p^2), \tag{10}$$

where p is the pixel scale in arcsec. The corresponding propagated error is

$$\sigma_\mu = \frac{2.5}{\ln 10}\cdot\frac{\sigma_s}{|s_{med}|}. \tag{11}$$

2.6. *Seeing (FWHM)*

The seeing was estimated for each target (through each filter) by selecting 8 isolated, not saturated stars and then computing a 2D image moment, and converting to FWHM following the Gaussian,

$$\mathrm{FWHM} = \sqrt{8\ln 2}\cdot\sqrt{\sigma_x\sigma_y}, \tag{12}$$

with σ_x, σ_y the second-moment widths in each axis. The per-filter FWHM values we report are the median of the 8 measurements and the uncertainty is the standard diviation across the same set of samples. See 4 for a discussion of how this approach overestimates the true FWHM of the sources in our data.

2.7. *Calibrated magnitudes and CMD construction*

For each source the calibrated apparent magnitude in filter f is

$$m_f = -2.5\log_{10}(F_f/t_{exp}) + m_{zp,f}, \tag{13}$$

with combined photon-noise and zero-point uncertainty

$$\sigma_{m_f} = \sqrt{\left(\frac{2.5}{\ln 10}\frac{\sigma_F}{F}\right)^2 + \sigma^2_{zp,f}}. \tag{14}$$

For CMD plotting we keep sources with SNR > 5 in B, V, and I. Note that Color-magnitude diagrams use V vs. $B-V$; color-color diagrams use $V-I$ vs. $B-V$.

2.8. *Isochrone overlay*

PARSEC isochrones A. Bressan et al. (2012) at $\log(\mathrm{age/yr}) = 7, 8, 9, 10$ (10 Myr, 100 Myr, 1 Gyr, 10 Gyr) were taken from the iscochrone.bat files supplied. To compare standard theoretical isochrones to our observed isochrones, we have to place them in the same rest frame as our clusters. Each isochrone is shifted by the cluster's distance modulus $\mu = 5\log_{10}(d/10\,\mathrm{pc})$ and reddened by the assumed $E(B-V)$ via the standard $R_V = 3.1$ extinction law (so $A_V = 3.1\,E(B-V)$). We use $d = 2.3$ kpc, $E(B-V) = 0.55$ for NGC 884 T. Currie et al. (2010), and $d = 0.4$ kpc, $E(B-V) = 0.60$ for the ONC L. A. Hillenbrand (1997).

3. RESULTS

3.1. *Detector characterisation*

The measured read noise and dark current for the two observing sessions are: NGC 884 $\sigma_{RN} = 14.82$ e$^-$/pix, $D = +0.057$ e$^-$/pix/s; ONC $\sigma_{RN} = 14.99$ e$^-$/pix, $D = +0.041$ e$^-$/pix/s. The dark current values are small but nonzero, and the read noise dominates in each frame since the CMOS being cooled to -5 C has such little contributions from dark current.

3.2. *Seeing*

The image-moments FWHM (Table 3) is approximately 6–7 pixels in NGC 884 (3-5 arcsec at $0.51''$/pix) and 9–11 pixels in the ONC (3.5-6 arcsec at $0.32''$/pix). Figure 2 overlays the V-band detections on the master frames.

3.3. *Photometric zero-points*

Per-filter zero-points are listed in Table 4. NGC 884 zero-points are 18.84, 18.62, 18.73, 17.01 mag for B, V,

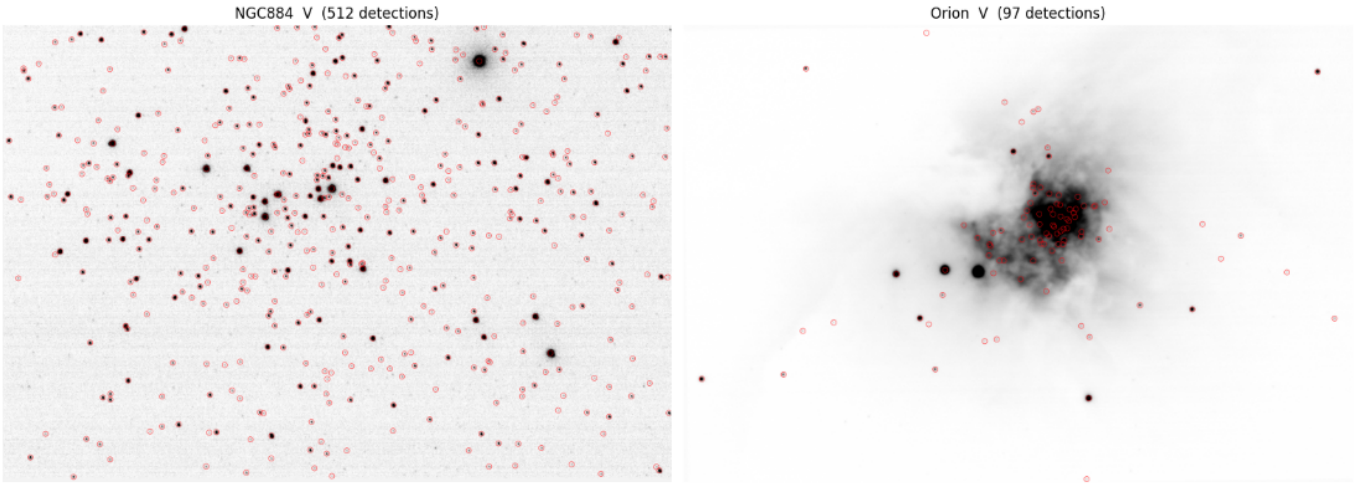


Figure 2. V-band master frames with DAOStarFinder detections marked in red. NGC884 is the left image and ONC is the Right image. The smaller ONC catalogue reflects the brighter sky background and the smaller field of view at the 14-inch.

Table 3. Image-moments FWHM per target per filter, in pixels and arcseconds. Reported uncertainties are the standard deviation across 8 stars.

Target	Filter	FWHM (pix)	σ (pix)	FWHM ($''$)
NGC 884	B	6.57	0.29	3.35
NGC 884	V	6.80	0.34	3.46
NGC 884	R	6.48	0.32	3.30
NGC 884	I	7.28	0.29	3.71
Orion	B	10.12	1.22	3.64
Orion	V	9.93	1.71	3.57
Orion	R	10.96	1.82	3.95
Orion	I	9.40	1.53	3.38

Table 4. Per-target / per-filter photometric zero-points.

Target	Filter	N_*	m_{zp}	σ_{zp}
NGC 884	B	4	18.84	0.25
NGC 884	V	4	18.62	0.13
NGC 884	R	1	18.73	0.01
NGC 884	I	1	17.01	0.01
Orion	B	3	19.46	0.37
Orion	V	3	19.53	0.24
Orion	R	3	19.41	0.22
Orion	I	3	18.11	0.51

R, I; Orion zero-points are 19.46, 19.53, 19.41, 18.11 mag. The Orion zero-points are $\sim$ 0.5–1 mag brighter than NGC 884 in B, V, R because the 14-inch telescope has a larger aperture and thus a larger collecting area than the 11-inch.

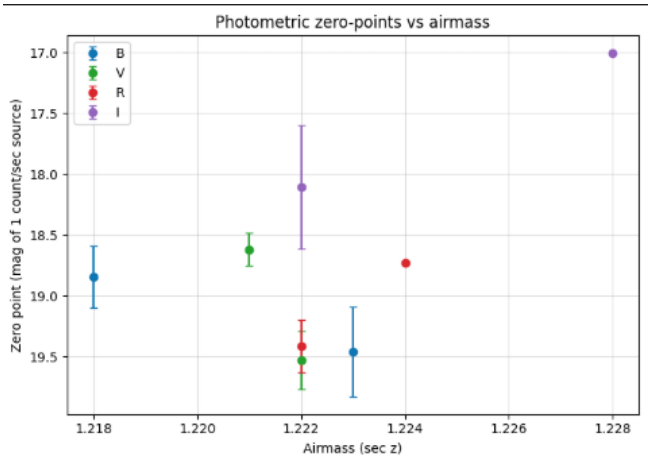


Figure 3. Per-filter photometric zero-points versus airmass. Errorbars show σ_{zp}.

The plot of zero-point versus airmass (Figure 3) shows no significant arimass dependence in our data because all observations were taken at similar airmass. The difference between the two clusters is likely dominated by the chaneg of telescope between observations as well as night-to-night transparency differences.

We foudn that the zero-point uncertainty ranged from $\sim$ 0.13 mag (NGC 884 V, 4 calibrators) to $\sim$ 0.5 mag (Orion I, 3 calibrators), excluding the single-star NGC 884 R, I cases whose 0.005–0.008 mag errors are a result of the lack of catalog reference data.

3.4. *Sky brightness*

Sky surface brightness for each observation is reported in Table 5. Values range from $\sim$ 19.6 mag/arcsec^2 (Orion R) to $\sim$ 22.9 mag/arcsec^2 (NGC 884 I). The

Table 5. Sky surface brightness in magnitudes per arcsec^2 and ADU per pixel.

Target	Filter	ADU/pix	μ (mag/arcsec^2)	Az (°)
NGC 884	B	10.5	20.98	331
NGC 884	V	13.6	20.47	331
NGC 884	R	12.1	20.71	331
NGC 884	I	0.5	22.94	330
Orion	B	17.7	19.86	185
Orion	V	13.6	19.83	184
Orion	R	14.8	19.62	183
Orion	I	1.6	20.72	184

two observing nights show that the NGC884 sky was darker than the sky near Orion. The reason we see this difference is largely in part of the extended emission of the Orion Nebula covering the entire frame. This means that our sky measurements actually include some emission from the nebula despite it being small.

The sky-brightness vs. airmass and azimuth panels (Figure 4) make this most directly visible. In the sky-brightness, azimuth comparison we can see ONC shows a greater sky background that NGC884.

3.5. *Calibrated photometry catalogue*

The full per-source calibrated photometry tables were collected and saved as CSV files, presented in the appendix as they are very large. Each row contains the source pixel position, the aperature flux measurement and uncertainty, the SNR, calibrated apparent magnitude, and per-star per-filter magnitude uncertainty. After we limited our stars to SNR > 5 in B, V, I, 415 NGC 884 sources and 95 ONC sources are left for the CMD. The Orion catalogue is smaller because of the brighter sky background (lowering the SNR floor) and the smaller field of view given the 3556 mm focal length.

3.6. *Zero-point validation*

To check our photometric calibration we picked 3 stars in each frame that were bright but not saturated, and importantly not used for zero-point calibration, and then compared our measured BVI magnitude to the BVI given in catalogs. We pulled their published BVI magnitudes from the Tycho-2, and APASS surveys via the Vizier catalog via Simbad(Table 6). For NGC884, the rsiduals were at worst 0.17 mag and consistent across filters. For ONC, the residuals were larger, around 0.3-0.7 mag, and the third object shows a residual of more than 4 mag. We believe this 4th object likely had a different catalog code than the one returned from the RA, Dec query(the selected code or star was not the one recieved from the catalog). Excluding that ourlier, the ONC measurements are generally consistent with their catalog values.

3.7. *Color images*

The R, V, B master frames for each cluster were assigned to the red, green, and blue channels of an RGB image and stretched as in Lab 4. NGC 884 (Figure 5) shows the dense bluish-white stars in the cluster core as well as the less dense star field around it. The ONC (Figure 6) shows the bright core of the orion nebula and the embedded ONC.

3.8. *Color–magnitude and color–color diagrams*

The four-panel diagram in Figure 7 shows the V vs. $(B-V)$ CMD and the $(V-I)$ vs. $(B-V)$ colour–colour diagram for each cluster.

For NGC884, the CMD shows a very nice clear vertical main sequence, broader pre-main-sequence buldge, as well as a red-giant turn off near the top. It extends from V ≈ 12 at the bright end down to $V \approx 18$ at the faint end. The color-color diagram shows a unredded star track with most stars consistent with a single intrinsic color curve. There is slight broadening by photometric scatter and patches of differential reddening across the cluster. The red, faint stars that lie of the CMD line and off the main focus of the color-color plot are likely faint background stars that are not members of the clutster.

For the ONC, the CMD is much less defined and lacks a clear main sequence such as in NGC884. Most stars are above and to the right of the zero-age main sequence with an ascending group of stars to the left of the main sequences. This is consistent with the dust extinction, excess heat, and pre-main-sequence behavior of hot young stars in embedded clusters. The color-color diagram is also more dispersed than that for NGC884. The color-color plot for ONC shows patchy reddening across the cluster and a high fraction of intrinsic color variation in the young, accreting, partially obscured stars.

3.9. *Isochrone fits and cluster ages*

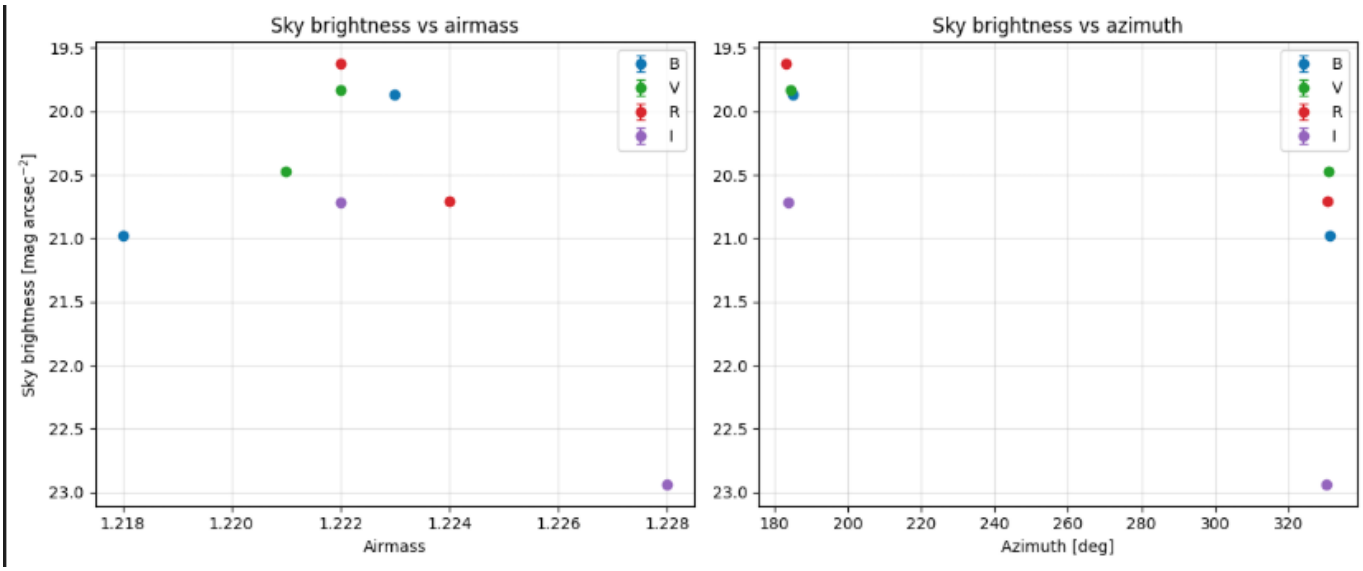


Figure 4. Sky surface brightness in mag/arcsec^2 versus airmass (left) and azimuth (right) per filter.

Table 6. Zero-point values are validated by comparing the catalog and measured BVI for stars not used as calibrators. Residuals are given by $\Delta = m_{\rm meas} - m_{\rm cat}$.

Cluster	TYC	cat B	meas B	ΔB	cat V	meas V	ΔV	cat I	meas I	ΔI
NGC 884	3694-1623-1	6.89	6.91	+0.02	6.45	6.41	−0.04	—	5.67	—
NGC 884	3694-1680-1	8.34	8.40	+0.05	8.10	8.05	−0.05	—	7.67	—
NGC 884	3694-1707-1	10.13	10.03	−0.10	9.81	9.64	−0.17	—	8.98	—
Orion	4774-934-1	6.10	6.18	+0.09	6.20	6.53	+0.33	—	6.66	—
Orion	2390-1411-1	8.81	8.12	−0.69	8.74	8.35	−0.39	—	8.33	—
Orion	4774-906-1	7.13	12.23	+5.11	6.93	11.75	+4.82	6.33	10.57	+4.24

For NGC 884 (Figure 8) the observed main sequence and red giant turn off falls bvetween the 10 Myr and 100 Myr PARSEC isochrones, with the data closer to the 10 Myr track at the bright end where the turnoff is most informative. This places the cluster age in the range $\tau \approx$ 10–30 Myr. This is consistent with the literature age of $\sim$ 14 Myr T. Currie et al. (2010).

For the ONC (Figure 9) estimating the age is more challenging. The youngest available isochrone in our PARSEC table is 10 Myr; this is already too old to bracket the actual ONC age of $\sim$ 1–3 Myr from below. At the assumed distance modulus and reddening the 10 Myr isochrone passes through approximately the lower edge of the observed PMS grouping, so we can only place an upper limit $\tau \lesssim$ 10 Myr from this CMD. The literature value of $\sim$ 1–3 Myr L. A. Hillenbrand (1997), cementing the inconclusiveness of the comparison with these isochrones.

4. DISCUSSION AND ERROR ANALYSIS

Zero-point calibration. For NGC 884 R and I, only one calibrator is available because three of our four bright Tycho-2 standards are above APASS's $V \sim 10$ saturation limit and Tycho-2 itself does not carry R or I. The σ_{zp} of $\sim$ 0.005 mag reported for those filters is the photon-noise error on that one star and is not a real estimate of the zero-point uncertainty. Doing this lab again, one could correct this by only selecting reference standard stars that are dimmer than APASS's cutoff magnitude.

Distance modulus and reddening. Both adopted distances and $E(B-V)$ values are taken from prior literature on the clusters. Uncertainties are at the level of $\Delta\mu \sim 0.1$ mag and $\Delta E(B-V) \sim 0.05$. These errors translate into vertical and horizontal shifts of the isochrones on the CMD that are close to the photometric scatter,thus dominating the uncertainty on the cluster age.



Figure 5. Reduced, aligned, and median-stacked RGB color image of NGC 884. Stretched with a midtones transfer function and histogram clip.

Isochrone grid. The available PARSEC table samples log(age) at 1.0-dex intervals (10 Myr, 100 Myr, 1 Gyr, 10 Gyr). Having so few isochrones makes it challenging to more percisely estiamte the age of the clusters, especially the ONC as it is significantly younger than the 10 Myr isochrone.

Sky-brightness comparison. The two observations are at the same airmass but different telescopes, different nights, different azimuths, different targets, and different fields of view. We conclude that the difference is sky background is primarily associated with the extended emission of the ONC and surrounding Orion Nebula as well as due in part to increased light pollution at that azimuth.

Crowded-field cross-matching. The zero-point validation showed one obvious outlier (TYC 4774-906-1 in the ONC) where the nearest-neighbour matching of TSV positions to detections returned the wrong star. Since the stars were identified by plate solving the images then querying around the measrued center of the star, star center measruement errors and the inability to detect other fainter stars in the air led to the misidentification. To fix this, following the plate solve if we utilize the wcs file created we may be able to get a more accurate measurement of the star center than is possible by hand.

5. CONCLUSION

In this Lab we preformed the full data reduction and photometric reduction on two open star clusters, NGC884 and the ONC. For this we used data taken across two observing sessions at CTO taken on the 11-inch and 14-inch, for NGC884 and the ONC respectively. Hand-picked Tycho-2 standard stars were used to calculate the per-filter zero-point offsets, calibrating our photometric measurements to an uncertainty of 0.1-0.3 mag. The sky brightness was characterized by sampling areas of the frame with intensities lower than 60% of the frame. This yielded a sky brightness measurement ranging from 19.6-22.9 mag/arcsec^2. We constructed

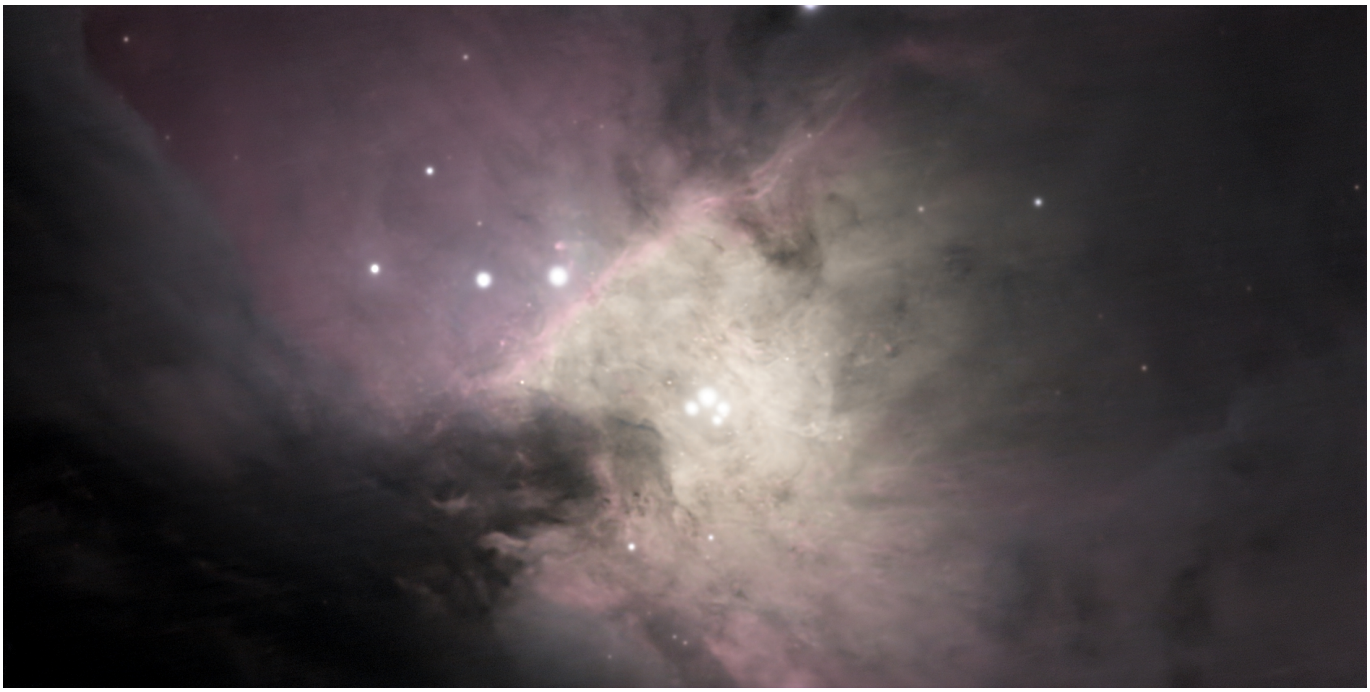


Figure 6. Reduced, aligned, and median-stacked RGB color image of the ONC. Stretched with a midtones transfer function and histogram clip.

two CMD plots, one for each cluster, overplotted standard reference isochrone, and were able to estiamte the ages of both clusters to 15 Myr for NGC884 and ≤ 10 Myr for ONC.

Specifically, Isochrone fits placed the NGC 884 age at $\sim$ 10–30 Myr, broadly consistent with the literature value of 14 Myr although limited by the coarse 1-dex isochrone grid available. Additionally, for the same reason we were only able to place only an upper limit $\tau \lesssim 10$ Myr on the ONC pending the addition of younger isochrones to the grid. The lab built directly on the data-reduction pipeline from Lab 4 and added a complete photometric workflow on top: per-pixel uncertainty propagation through every step, source detection and aperture photometry, calibration against catalogue standards , sky-background characterization, seeing measurement, and zero-point validation with catalogue stars.

If we were to repeat this lab, the most useful single change would be to plate-solve the science frames with `astrometry.net` and utilize the WCS frame it creates. This would allow us to replace the nearest-neighbour querying with WCS-based catalogue source matching. Beyond that, downloading a finer isochrone grid (log age = 6.0, 6.5, 7.0, 7.5, 8.0, ...) and switching the seeing measurement from image moments to a 2D Gaussian profile fit would tighten both the age and the spatial-resolution numbers reported here.

REFERENCES

Bressan, A., Marigo, P., Girardi, L., et al. 2012, PARSEC: stellar tracks and isochrones with the PAdova and TRieste Stellar Evolution Code, MNRAS, 427, 127, doi: 10.1111/j.1365-2966.2012.21948.x

Currie, T., Hernandez, J., Irwin, J., et al. 2010, The Stellar Population of h and χ Persei: Cluster Properties, Membership, and the Intrinsic Colors and Temperatures of Stars, ApJS, 186, 191, doi: 10.1088/0067-0049/186/2/191

Henden, A. A., Levine, S., Terrell, D., & Welch, D. L. 2015, APASS – The Latest Data Release, AAS Meeting Abstracts, 225, 336.16

Hillenbrand, L. A. 1997, On the Stellar Population and Star-Forming History of the Orion Nebula Cluster, AJ, 113, 1733, doi: 10.1086/118389

Høg, E., Fabricius, C., Makarov, V. V., et al. 2000, The Tycho-2 catalogue of the 2.5 million brightest stars, A&A, 355, L27

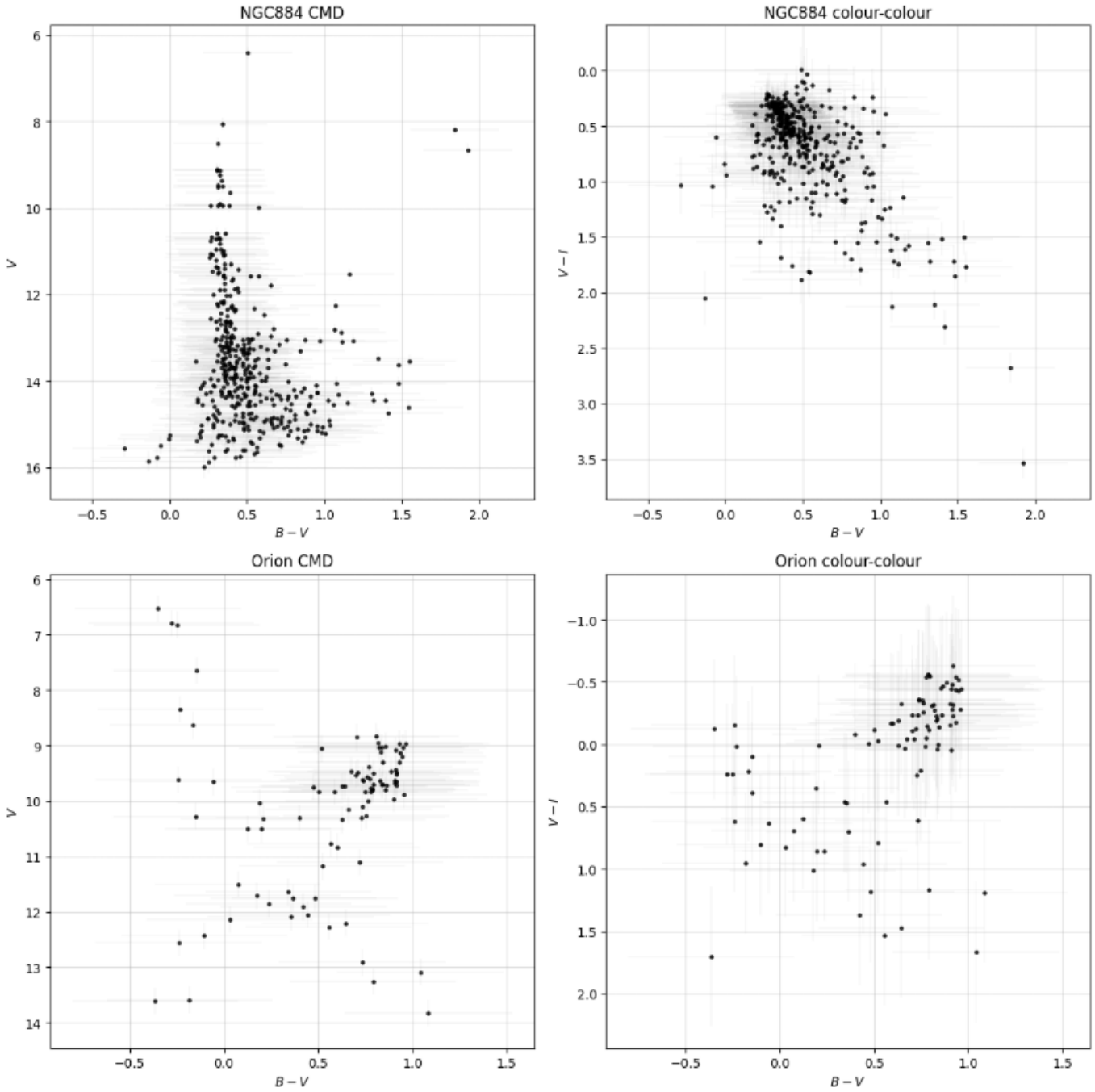


Figure 7. Top left: NGC 884 V vs. $B-V$ CMD. Top right: NGC 884 $V-I$ vs. $B-V$ colour–colour diagram. Bottom: same for the ONC.

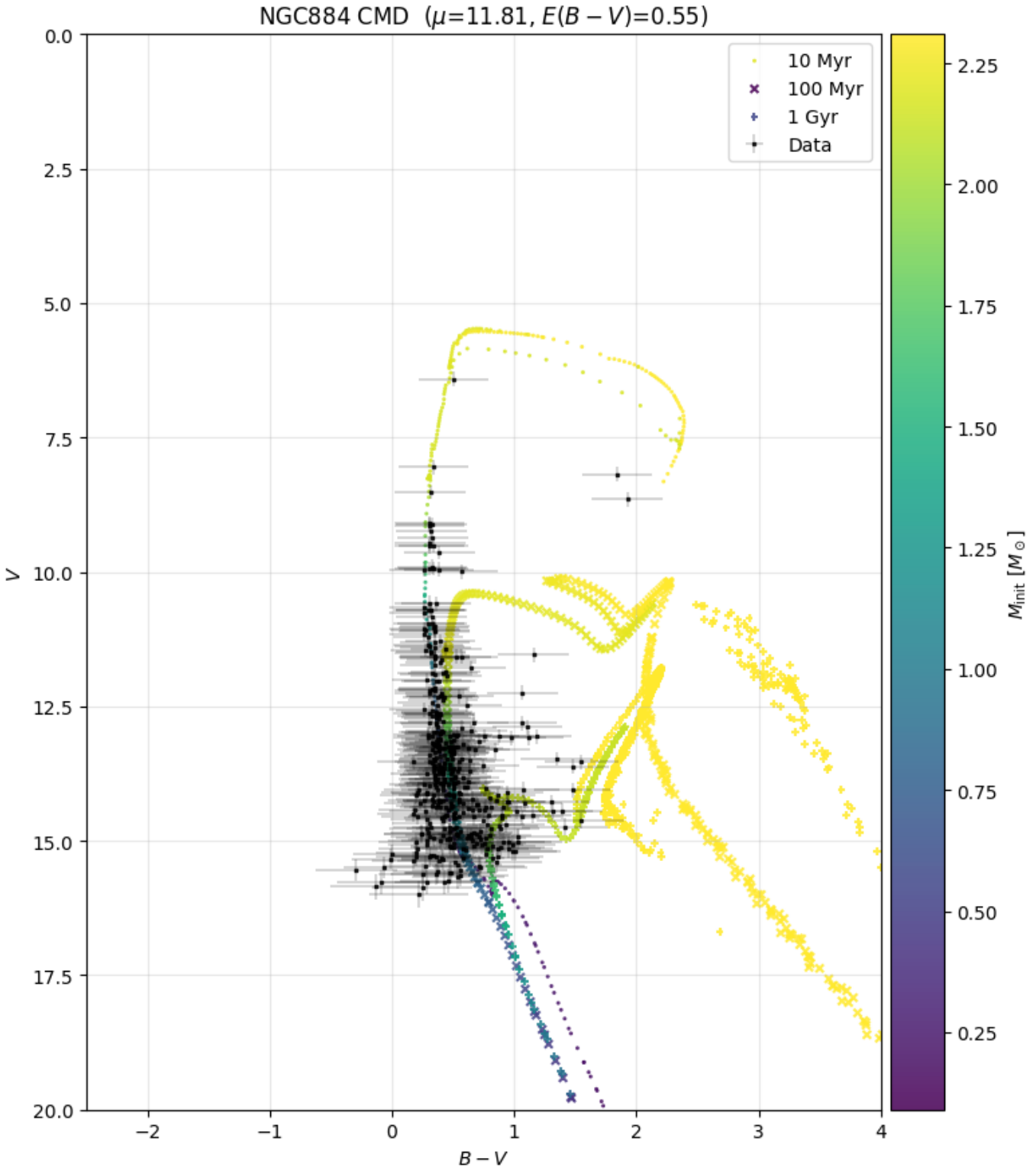


Figure 8. NGC 884 V vs. $B-V$ CMD overlaid with PARSEC isochrones at 10 Myr, 100 Myr, and 1 Gyr. Isochrones are shifted by $\mu = 11.81$ mag and reddened by $E(B-V) = 0.55$, $A_V = 1.71$.

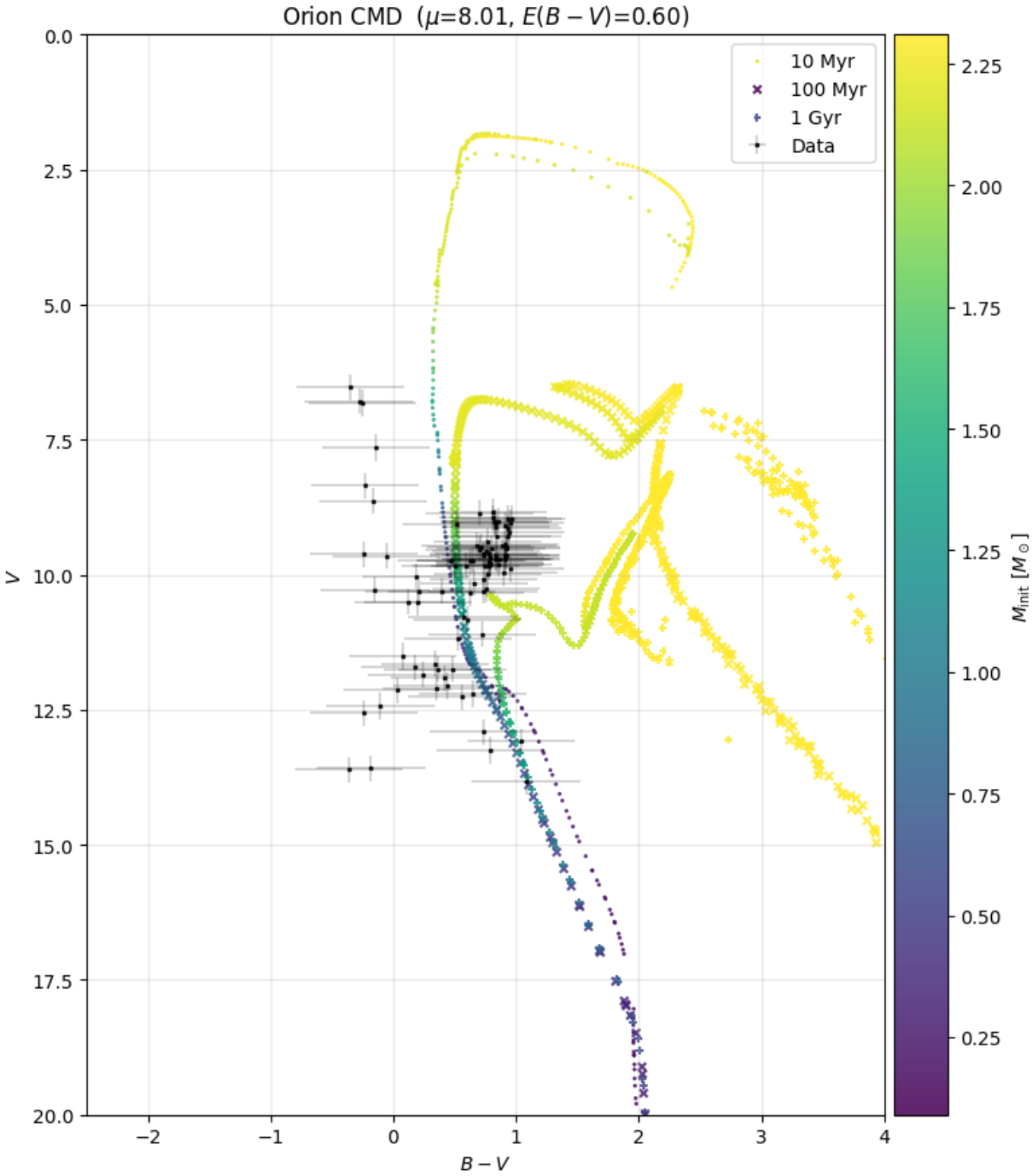


Figure 9. Orion Nebula Cluster V vs. $B-V$ CMD overlaid with PARSEC isochrones at 10 Myr, 100 Myr, and 1 Gyr. Isochrones are shifted by $\mu = 8.0$ and reddened by $E(B-V) = 0.60$.